CDF/PUB/EXOTIC/PUBLIC/9166

Neural Network Search for Standard Model Higgs Boson in $\not\!\!E_T$Plus Jets Channel with 1.7 fb^{-1}

The CDF Collaboration
URL http://www-cdf.fnal.gov
(Dated: January 17, 2008)

This analysis focuses on a low mass Higgs boson search with 1.7 fb^{-1} of data. We look for Higgs events in which it is produced in association with a W or Z boson for either a Z$\rightarrow \nu\nu$ decay or a leptonic W decay in which the lepton goes undetected. Such events are expected to leave a distinct signature of large missing transverse energy, as well as jets with taggable secondary vertices from the H$\rightarrow b\bar{b}$ decay. Utilizing a new track based technique for removing QCD multijet processes in addition to a neural network discriminant, we calculate an expected limit of 8.3 times the Standard Model prediction at the 95% CL for a Higgs boson mass of 115 GeV/c^2, with an observed limit of 8.0*SM.

Preliminary Results for Winter 2008 Conferences

I. INTRODUCTION

The Higgs boson is the sole remaining undiscovered piece of the Standard Model of particle physics. While the Higgs mechanism is a fundamental component of Electroweak unification, the observable Higgs boson has eluded all experimental measurements. The mass of this particle is not predicted by theory, but experimental studies performed at LEP have constrained the mass range. Analysis of data from ALEPH, DELPHI, L3, and OPAL set a lower mass limit of 114.4 GeV/c^2. In addition, increasingly accurate measurements of the top quark as well as electroweak observables constrain the upper mass limit on the Standard Model Higgs boson to 144 GeV at the 95% confidence level [1, 2]. This analysis will focus on a Higgs boson search in this mass region of 110-150 GeV/c^2.

In proton-antiproton collisions at the Tevatron, a standard model Higgs boson may be produced in association with a Z or W vector boson [3]. Events in which the Z decays to undetectable neutrinos, leave a distinct signature of missing energy in the transverse direction($\not\!\!E_T$). This particular channel also expects a significant amount of signal yield from WH events in which the W decays leptonically, but the high P_T lepton is not identified by the orthogonal WH search. These events often have large $\not\!\!E_T$as well. Models of the signal as well as most backgrounds are developed using Monte Carlo. However, the largest background contribution in this analysis involves the QCD production jets, and this background is modeled directly from the data.

II. DATA SAMPLE & EVENT SELECTION

The data sample utilized in this analysis was collected on a missing transverse energy plus two jets trigger, and is comprised of a total integrated luminosity of 1.7 fb^{-1}. A $\not\!\!E_T$threshold of 50 GeV is applied to the data sample to account for trigger inefficiencies and rising background rates at low $\not\!\!E_T$. Additional event selection is made to account for other trigger inefficiencies or background rejection.

- A leading jet requirement of $|\eta| < 2.0$ and $E_T > 45$ GeV and second jet requirement of $|\eta| < 2.0$ and $E_T > 25$ GeV is placed on all events.
- Either the lead or second jet must be central($|\eta| < 0.9$) due to trigger requirements.
- Events are vetoed if a third jet exists with $|\eta| < 2.4$ and $E_T > 20$ GeV.
- Lead and second jet are required to be separated by $\sqrt{\Delta\phi^2 + \Delta\eta^2} > 1.0$.
- Exclude region where $\Delta\phi(\not\!\!E_T$-Lead Jet) < 0.8. This cut is highly efficient for signal, and removes a small amount of background.
- Events with identified high-energy electrons and muons are not accepted, as these are potential candidates for orthogonal WH searches.
- The data sample is divided into a signal sample where $\Delta\phi(\not\!\!E_T$-2nd Jet) > 0.8 and a QCD control sample where the missing E_T is aligned with the second jet($\Delta\phi(\not\!\!E_T$-2nd Jet) < 0.4).

A. Tagging Algorithms

To isolate a data sample that is enriched with physics involving b quarks, algorithms are implemented to locate secondary vertices consistent with the long lifetime of b-hadrons. This method has been used in other Higgs searches and top analyses [4]. An additional jet probability algorithm is implemented by requiring a low probability that all tracks in a jet are consistent with originating from the primary vertex [5]. The data sample is therefore split into events in which both jets satisfy the secondary vertex tagging algorithm, and events in which one jet is secondary vertex tagged, while the other satisfies the jet probability requirement.

III. SIGNAL AND BACKGROUND PREDICTION

A. ZH$\rightarrow \nu\nu b\bar{b}$ and WH$\rightarrow (l^{\pm})\nu b\bar{b}$

Signal Monte Carlo samples were generated with the PYTHIA program [8] for Higgs masses between 110-150 GeV/c^2. The expected event yield of the signal is predicted according to its efficiency for passing event selection,

b-tagging requirements and trigger parameterization. This overall efficiency is then used to calculate the total signal prediction resulting from the standard model theoretical cross section times braching ratios for 1.7 fb^{-1} of data in proton-antiproton collisions at $\sqrt{s}$ =1.96 TeV.

	$ZH \rightarrow \nu\nu b\bar{b}$		$WH \rightarrow l\nu b\bar{b}$	
Mass	Vertex + Probability Tag	Double Vertex Tag	Vertex + Probability Tag	Double Vertex Tag
110	0.63	0.78	0.46	0.57
115	0.54	0.68	0.41	0.49
120	0.46	0.59	0.32	0.39
130	0.30	0.38	0.21	0.25
140	0.17	0.20	0.10	0.14
150	0.07	0.08	0.04	0.05

TABLE I: *Mean signal event expectations in 1.7 fb^{-1} after event selection and b-tagging*

B. Background Modeling

Most backgrounds to the physics of interest in this analysis are modeled with Monte Carlo. The W/Z + heavy flavor($b\bar{b}, c\bar{c}, c$) backgrounds were generated by the ALPGEN program interfaced with PYTHIA which provides the parton showering [7, 8]. These background predictions are scaled relative to other CDF measurements utilizing the method outlined in Ref. [4]. Diboson, $t\bar{t}$ and single top background expectations are calculated according to their theoretical or measured cross sections.

The falsely tagged light flavor (mistag) background is predicted from the data by utilizing negatively-tagged events, events in which the measured displacement of the secondary vertex is opposite the b jet direction. These tags are due to limitations in resolution, as are events in which light flavor jets are associated with a secondary vertex. The negative tag prediction is scaled by an asymmetry factor to predict the amount of light flavor for a particular set of event cuts and tagging algorithms.

Validation of electroweak and top backgrounds are performed in events with one isolated high P_T muon. The $\not\!\!E_T$is not corrected for the presence of the muon to simulate the effect of an additional neutrino. A requirement of at least one secondary vertex tag is made, as well as the same event selection required for the signal region other than the muon veto. The background model reproduces the data well, as seen if Figure 1.

1. *Heavy Flavor QCD*

The single largest background to the Higgs signal in the $\not\!\!E_T$+ jets channel involves heavy flavor QCD jet production. This background is typically the result of $\not\!\!E_T$being generated by calorimeter mismeasurement, although $\not\!\!E_T$can also be generated by semi-leptonic decay in heavy flavor jets. The majority of this background is removed by requiring that the $\not\!\!E_T$not be aligned with the lower transverse energy jet, which we refer to as the second jet. However, the region in which the $\not\!\!E_T$is aligned with the second jet is used as a control region to test the kinematic shapes of the heavy flavor QCD model. The QCD model is taken directly from the data in events with one and only one secondary vertex tag. The single mistagged light flavor background shape is subtracted out of the data, and biases introduced by tagging are applied to the untagged jet. The resulting shape contains almost entirely heavy flavor physics processes producing bottom and charm quarks, with relevant instrumental effects and biases applied. Good agreement is shown between the data and QCD model for the many kinematic and topological distributions studied in the QCD dominated region where the $\not\!\!E_T$is aligned with the second jet, as seen in Figure 2. After validating the method in this region, a similar procedure is applied to the signal region by subtracting mistag, electroweak and top quark processes out of the single tag data. The resulting shape is used to model the QCD background in validation plots or for the discriminant used in limit calculations. This procedure produces the shape of the QCD, but the normalization is allowed to float.

IV. ARTIFICIAL NEURAL NETWORKS

Two separate neural networks have been developed for this analysis. The first neural network is focused on separating a ZH signal from the QCD mutli-jet background. While the large $\not\!\!E_T$in a ZH event is driven by the Z$\rightarrow \nu\nu$ decay, the $\not\!\!E_T$in a QCD event is typically generated by mismeasurement of jets in the calorimeters. While

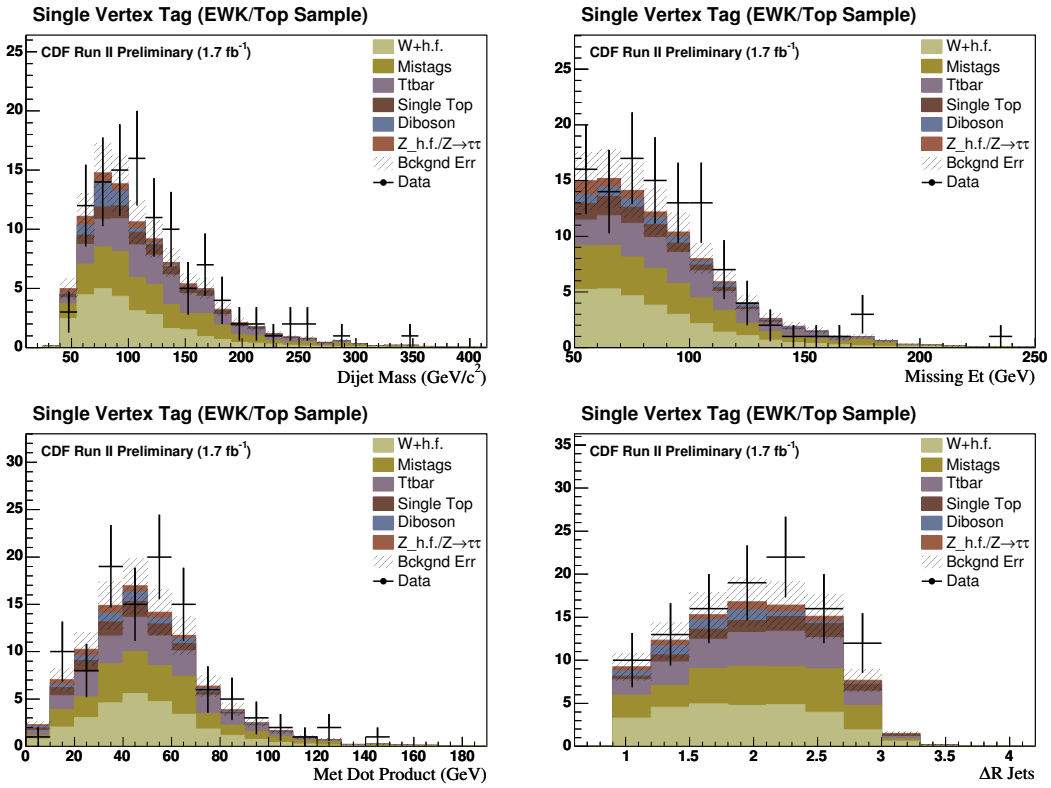

FIG. 1: Figures for at least one secondary vertex tagged jet with an identified high P_T muon. Upper left: Dijet Mass; upper right: Missing E_T; lower left: Met Dot Product; lower right: ΔR Jets.

	Vertex + Probability Tag	Double Vertex Tag
$t\bar{t}$	8.1 ± 1.5	8.2 ± 1.3
single top	4.5 ± 0.8	4.7 ± 0.8
WZ/WW	1.4 ± 0.3	1.2 ± 0.2
ZZ	2.0 ± 0.4	2.3 ± 0.4
W+h.f.	8.8 ± 3.8	6.9 ± 2.9
Z+h.f./Z→ $\tau\tau$	8.2 ± 3.6	8.0 ± 3.4
Mistags	8.3 ± 2.4	1.5 ± 0.3
Total non-QCD h.f.	41.3 ± 6.0	32.9 ± 4.8
QCD h.f. (Fit)	16.5 ± 10.7	16.4 +- 8.6
Total Background	57.8 ± 12.3	49.3 +- 9.8
Data	62	48

TABLE II: *Event expectations for background processes after signal region event selection. QCD normalization is estimated by fitting the final neural network QCD shape to the data.*

such mismeasurements typically fall into the QCD control regions where the $\not\!\!E_T$is aligned with the second jet, they can also mimic a signal-like topology, with the $\not\!\!E_T$pointing away from both identified jets. However, any missing energy that is the result of calorimeter mismeasurement is uncorrelated to the P_T of charged particles as measured in the tracking chamber. Conversely, the $\not\!\!E_T$in events with high energy neutrinos will be correlated with missing P_T from tracking information. Using a neural network, several track-based quantities are used to discern $\not\!\!E_T$caused by a high-energy neutrino from that resulting from calorimeter mismeasurement. This track-based discriminant is highly efficient at separating these two processes, solely using tracking information as shown in Figure 3.

A second neural network has been trained as a final discriminant which is used for limit calculations. The network has been trained to seperate ZH and WH signal from QCD and $t\bar{t}$ backgrounds. Using the previously described track-based discriminant as an input, as well as four additional inputs, network training was performed by the JETNET package [6], for the following quantities:

Track-based Discriminant: Neural Network trained with tracking information to separate fake from real $\not\!\!E_T$.

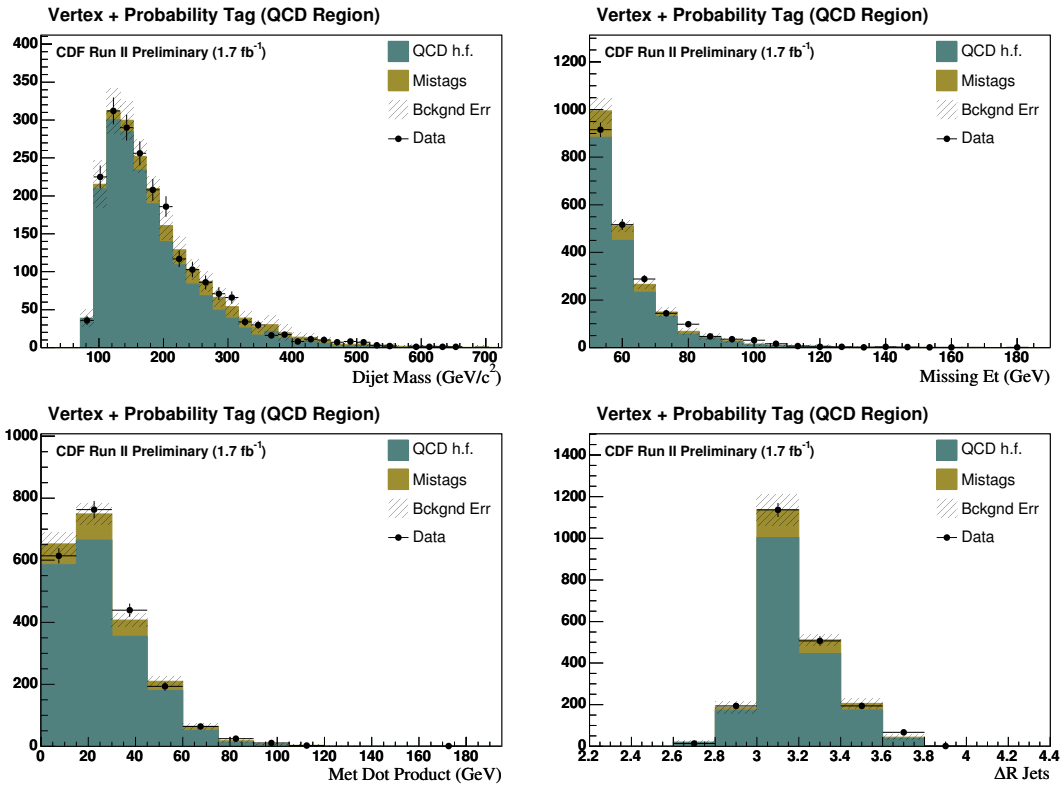

FIG. 2: Figures for 1 secondary vertex + jet probability tag in region where Missing E_T is aligned with second jet. Upper left: Dijet Mass; upper right: Missing E_T; lower left: Met Dot Product; lower right: ΔR Jets.

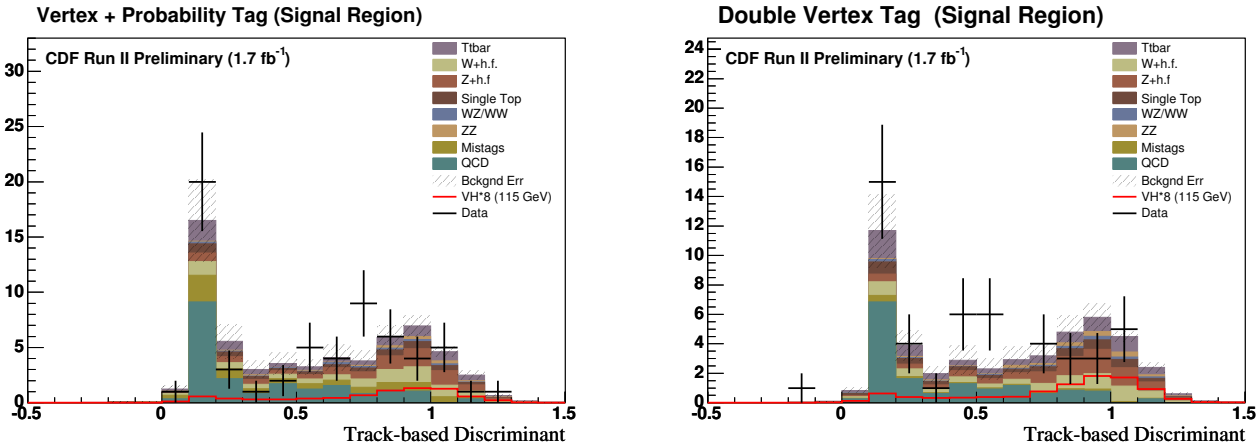

FIG. 3: Track-based Neural Network output for both double tag samples.

Dijet Mass: The invariant mass of the reconstructed dijet system.

Met Dot Product: The dot product of the calorimeter-based transverse missing energy direction combined with the track-based transverse missing energy direction.

Missing E_T: The $\not\!\!E_T$calculated from calorimeter information, taking into account corrections applied to jets in an event.

ΔR(Lead-2nd Jet): Seperation in η and ϕ of the lead and second jet.

Neural network shapes for various backgrounds are determined by running Monte Carlo through the neural network

Combined Double Tag Limits						
Higgs Mass	*a priori* limits					
(GeV/c^2)	-2σ	-1σ	median	$+1\sigma$	$+2\sigma$	Obs
110	3.7	5.2	7.4	10.7	15.1	9.6
115	4.3	5.8	8.3	12.1	17.0	8.0
120	5.1	7.0	9.9	14.4	20.6	9.5
130	7.8	10.7	15.3	21.9	30.6	12.8
140	13.0	17.8	25.1	35.9	49.9	20.0
150	32.8	44.5	63.3	91.3	129.2	44.3

TABLE III: The 95% CL limits as ratio over standard model expectation. Systematic errors are included in the calculation. The righthand column gives the observed limit with CDF's 1.7 pb^{-1} data sample.

after event selection. The QCD shape is taken directly from the data as previously described. While the network has been optimized to reduce QCD and $t\bar{t}$ backgrounds, it also provides good separation of the other backgrounds from Higgs signal. Individual neural networks were trained for 115 GeV/c^2 Higgs mass and mass points between 110-150 GeV/c^2 at intervals of 10 GeV/c^2 to optimize the sensitivity over a range of possible Higgs masses. Validation of the neural networks was performed in control region studies, as seen in Figures 9 and 8

V. SYSTEMATIC UNCERTAINTIES

Several sources of systematic uncertainty have been identified in this analysis. The largest uncertainty on the signal comes from the uncertainty on the scale factor assigned to b-tagging. This scale factor accounts for data-Monte Carlo differences. This scale factor is applied to all Monte Carlo backgrounds containing bottom or charm quarks. This uncertainty is 8.6% for the double vertex tag case and 9.1% for vertex plus probability tag normalizations. Uncertainties on initial and final state radiation vary between 1% and 5% for the signal. Additional uncertainties on all Monte Carlo backgrounds and signal include PDF (2.0%), lepton veto (2.0%) and luminosity (6.0%). Some systematics effect both the shape of distributions as well as normalization, such as jet energy scale, trigger parameterization uncertainty and uncertainties on the shape of data-driven QCD and mistag models.

VI. RESULTS

We perform a direct seach for a significant deviation in data shape from the background hypothesis. A binned maximum likelihood technique is used to calculate expected 95% confidence level limits. Individually trained neural network shapes are used in each limit calcuation for a particular Higgs boson mass. The output of the backgounds, signal and data are displayed in Figure 4. To extract the 95% confidence level limits, backgrounds are constrained within their uncertainties in pseudo-experiment studies. The two tagging classes are treated as independent samples, however, they have correlated systematic errors. The uncertainties for both normalization and shape systematics are considered in limit calculations. We set 95% confidence level limits in the mass range from 110-150 GeV/c^2. Table III shows the combined *a priori* 95% CL limits for both tagging categories, along with the $\pm 1\sigma$ and $\pm 2\sigma$ range of limits. These are presented as a ratio of the limit divided by the Standard Model cross section. The observed limit with the CDF data sample is shown in the final column of the table. These limits are plotted in Figure 5.

VII. CONCLUSIONS

This analysis searches for a standard model Higgs boson produced in association with Z and W bosons. Higgs is assumed to decay to $b\bar{b}$ quarks, and the Z to neutrinos, accounting for branching ratios. The acceptance from WH events comes from $W \rightarrow l\nu$ events, where the lepton is unidentified. The analysis introduces the use of a neural network as the primary discriminant, as well as a track-based neural network to discern fake from real $\not\!\!E_T$. Utilizing two separate double tag categories, we calculate an expected limit of 8.3 times the Standard Model prediction at the 95% CL, for a Higgs mass of 115 GeV/c^2, with an observed limit of 8.0*SM.

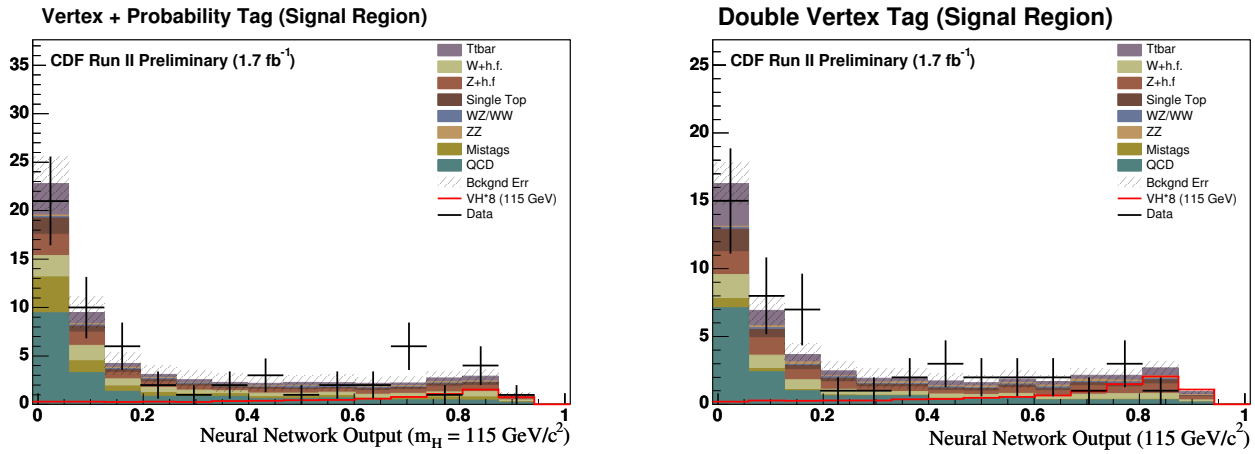

FIG. 4: Neural network output used to set limits on SM Higgs production. Left: Events with one secondary vertex tagged jet and one jet probability tagged jet; Right: Events with two secondary vertex tagged jets;

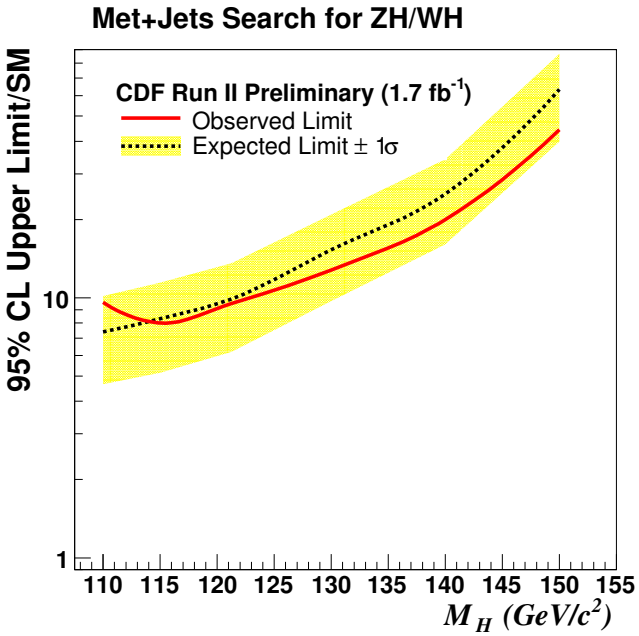

FIG. 5: 95% confidence level limits as a ratio over standard model VH expectation. Limits are are plotted as a function of Higgs boson mass.

Acknowledgments

We thank the Fermilab staff and the technical staffs of the participating institutions for their vital contributions. This work was supported by the U.S. Department of Energy and National Science Foundation; the Italian Istituto Nazionale di Fisica Nucleare; the Ministry of Education, Culture, Sports, Science and Technology of Japan; the Natural Sciences and Engineering Research Council of Canada; the National Science Council of the Republic of China; the Swiss National Science Foundation; the A.P. Sloan Foundation; the Bundesministerium für Bildung und Forschung, Germany; the Korean Science and Engineering Foundation and the Korean Research Foundation; the Particle Physics and Astronomy Research Council and the Royal Society, UK; the Russian Foundation for Basic Research; the Comision Interministerial de Ciencia y Tecnologia, Spain; and in part by the European Community's

Human Potential Programme under contract HPRN-CT-20002, Probe for New Physics.

[1] LEP Electroweak Working Group, `http://lepewwg.web.cern.ch/LEPEWWG/`
[2] ALEPH, DELPHI, L3, OPAL. The LEP Working Group for Higgs Boson Searches, Phys. Lett **B565** 61 (2003).
[3] T. Han and S. Willenbrock, Phys. Lett. **B273** (1991) 167;
A. Djouadi, J. Kalinowski, and M. Spira, Comp. Phys. Commun. **108 C** (1998) 56.
[4] A. Abulencia *et al.*, Phys. Rev. **D71**, 072005 (2005).
[5] D. Buskulic, *et al.* (ALEPH Collaboration), Phys. Lett. B **313**, 535 (1993);
F. Abe *et al.* (CDF Collaboration), Phys. Rev. D **53**, 1051 (1996);
A. Affolder *et al.* (CDF Collaboration), Phys. Rev. D **64**, 032002 (2001), Erratum-ibid: Phys. Rev. D **67**, 119901 (2003).
[6] L. Lönnblad, C. Peterson, and T. Rögnvaldsson, Comp. Phys. Comm. 81 (1994) 185.
[7] M.L. Mangano *et al.*, JHEP 0307:001, 2003.
[8] P. Edén, C. Friberg, L. Lönnblad, G. Miu, S. Mrenna, E. Norrbin, and T. Sjöstrand, Computer Phys. Commun. **135** (2001) 238.

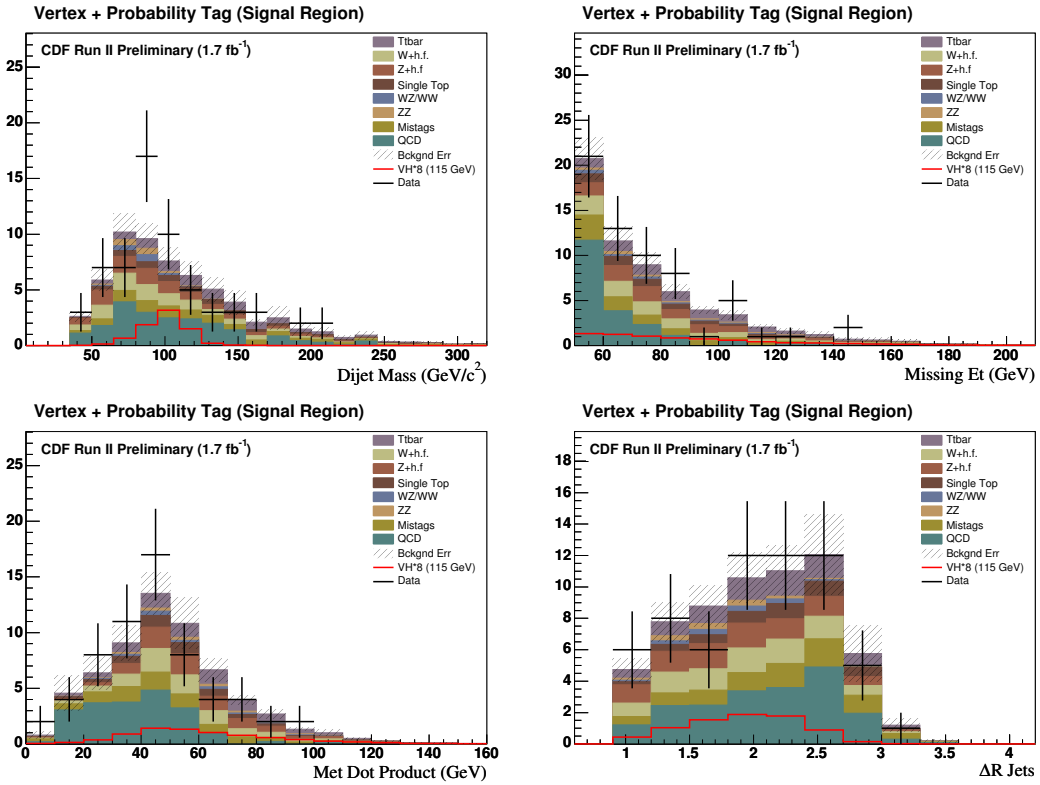

FIG. 6: Additional figures for 1 secondary vertex + jet probability tag in the signal region. Upper left: Dijet Mass; upper right: Missing E_T; lower left: Met dot product; lower right: ΔR(Lead-2nd Jet).

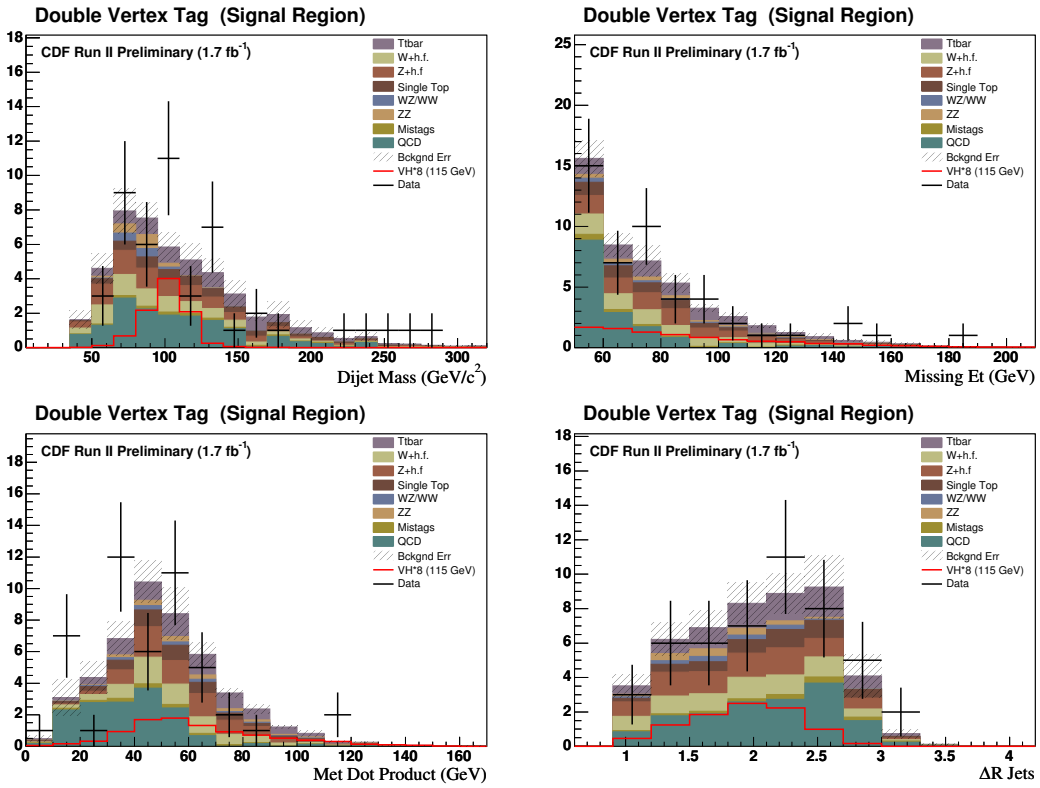

FIG. 7: Additional figures for 2 secondary vertex tags in the signal region. Upper left: Dijet Mass; upper right: Missing E_T; lower left: Met dot product; lower right: ΔR(Lead-2nd Jet).

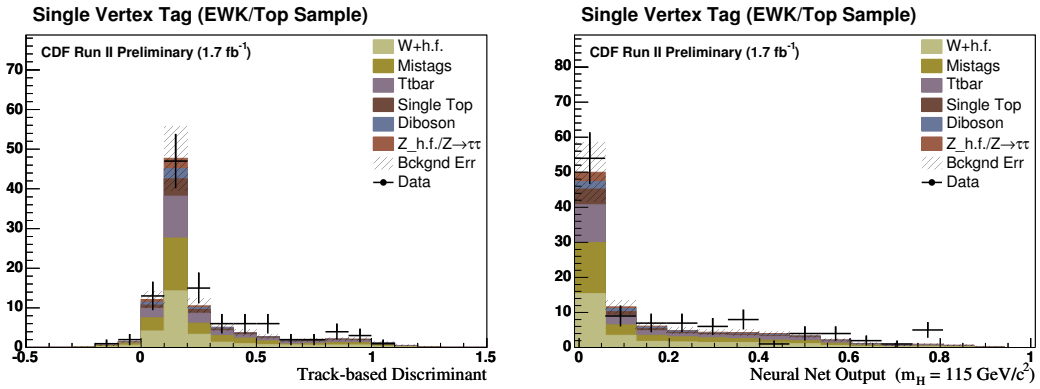

FIG. 8: Figures for at least one secondary vertex tagged jet with an identified high P_T muon. Left: Track-based Neural Network; Right: Neural Network Discriminant.

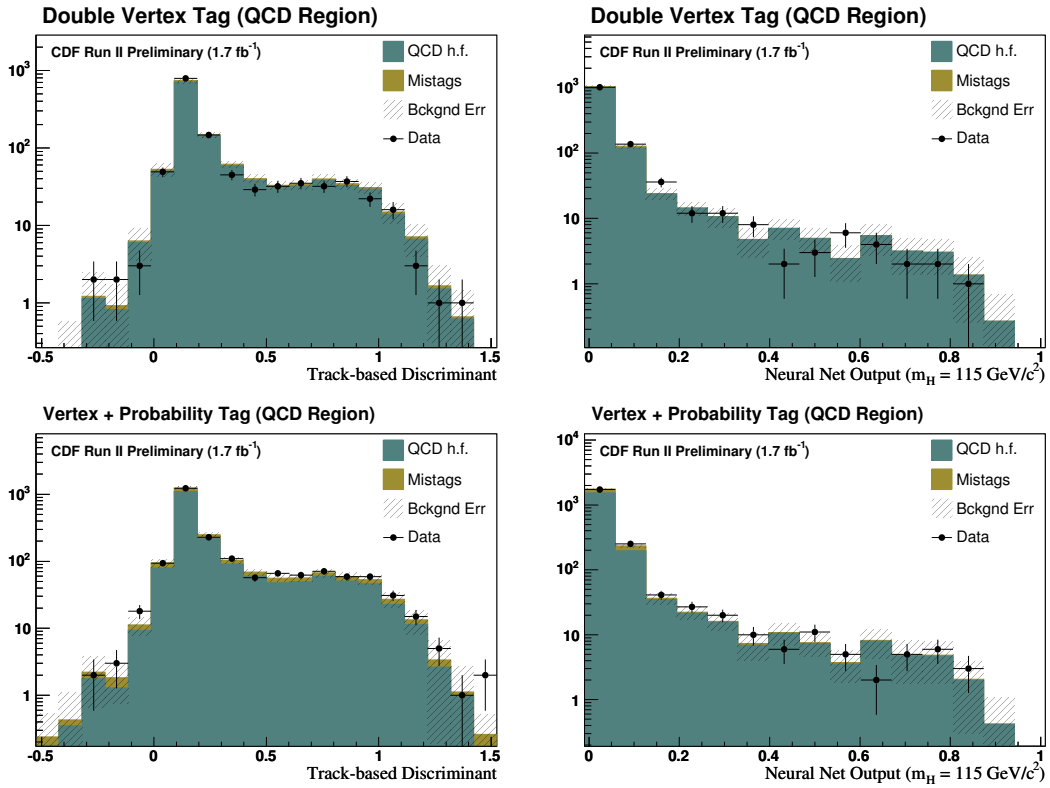

FIG. 9: Validation of multivariate techniques for 1 secondary vertex + jet probability tag in region where Missing E_T is aligned with second jet. Left: Track-based Neural Network; Right: Neural Network Discriminant.

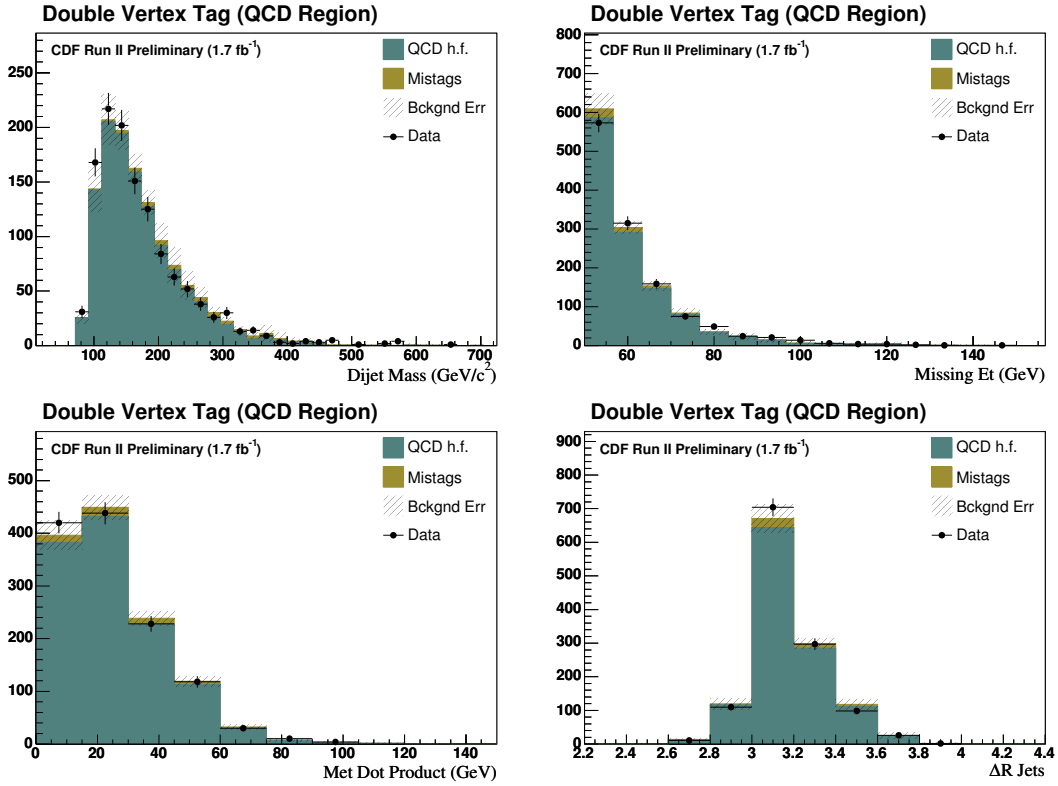

FIG. 10: Figures for 2 secondary vertex tags in region where Missing E_T is aligned with second jet. Upper left: Dijet Mass; upper right: Missing E_T; lower left: Met Dot Product; lower right: ΔR Jets.